International Applied Mechanics, Vol. 29, No. 9, 1993

PARAMETRIC RESONANCE IN THE SYSTEM: LIQUID IN TANK + ELECTRIC MOTOR

T. S. Krasnopol'skaya and A. Yu. Shvets

UDC 532.595:534.1

Resonance oscillations and waves in a liquid contained in cylindrical and spherical tanks (tanks with at least one angular coordinate) are adequately described by pendulum models [3, 5-8, 10-13]. The resonance phenomenon itself, i.e., dominant oscillations in one or more modes, can be used to reduce the investigation of continuous systems to low-dimensional models. This procedure is well known. What are its most important features from the standpoint of science today? First, it relegates the coupling of resonance modes with nonresonance modes to secondary status. Quantitatively, the equations describing resonance modes in terms of their coefficients are subject to the influence of nonresonance modes. However, the influence of instability of these modes on the dynamics of resonance modes is eliminated, so that the complexity of the problem is significantly diminished. Second, when this procedure is used in problems of fluid dynamics in a cylinder or a sphere, it distinguishes — as a minimum — equations for two "coupled" modes [4] having the same eigenfrequencies and corresponding to eigenfunctions in the angular coordinate θ of the form $\cos n\theta$ and $\sin n\theta$. When the eigenfrequencies corresponding to modes with different wave parameters are close to one another, this procedure [5] yields four equations, taking into account the coupling and mutual influence for resonance modes.

Mode coupling can be regarded as an avenue by which the investigated deterministic systems acquire strange attractors, because the averaged equation for one mode (not coupled with other modes) does not have stabilized states of the chaotic attractor type. For coupled modes, when a resonant excitation directly stimulates one mode (or in the case of oscillations of a spherical pendulum with the excitation of plane oscillations), the amplitude–frequency response of the excited mode has an additional region of instability besides the standard region. This new region is the result of instability of the zeroth solution of the second coupled mode, which is not excited directly. The existence in the system of a second mode, which has a resonance frequency but is not excited directly, can disrupt the stability of the oscillatory states in the first, directly excited mode. This phenomenon is clearly demonstrated in the pendulum model [10] and is observed in all distributed systems having an angular coordinate [2, 4, 12].

A third feature of the given procedure is its applicability for preliminary fluid-dynamic analysis when the oscillations of the tank are excited by different techniques in the spherical pendulum model. It has been shown [7, 11, 12] that the forced and parametric resonances associated with the oscillations of a liquid in tanks are described by different systems of equations having qualitatively different properties. A chaotic steady state, which cannot exist for parametric oscillations, is possible in the case of forced oscillations.

We have previously carried out a detailed analysis of the oscillations of a liquid in a cylinder, taking into account the effects of interaction with the energy source [3]. In this article we investigate the behavior of parametric resonance in the same mechanical system. We have two objectives in mind: to show that interaction with the excitation mechanisms can generate chaos and to demonstrate new attributes exclusive to parametric resonance.

We consider the mechanical system in Fig. 1. The shaft of an electric motor is connected through a slider-crank mechanism to a platform, on which is mounted a rigid cylindrical tank of radius R partially filled with a liquid. When the crank arm x_0 rotates through an angle σ, the platform acquires a displacement of the form $v(t) = x_0 \cos \sigma(t)$. To describe the oscillations of the free surface, we introduce cylindrical coordinates $Oxr\theta$, whose origin is located at the intersection of the tank axis with the undisturbed surface of the liquid. We can then write the equation for the relief of the free liquid surface in the form $x = \eta(r, \theta, t)$. We assume that the liquid is inviscid and incompressible, has a density ρ, and fills the cylindrical tank of cross section S to a depth $x = -d$.

Institute of Mechanics, Academy of Sciences of Ukraine, Kiev. Translated from Prikladnaya Mekhanika, Vol. 29, No. 9, pp. 52-61, September, 1993. Original article submitted March 26, 1992.

1063-7095/93/2909-0722$12.50

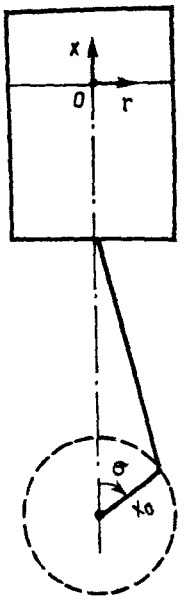

Fig. 1

We seek the relief function of the liquid surface as an expansion in eigenmodes [3]

$$\eta(r,\theta,t) = \sum_{i,j}\left[q_{ij}^{c}(t)\kappa_{ij}(r)\cos i\theta + q_{ij}^{s}(t)\kappa_{ij}(r)\sin i\theta\right]. \tag{1}$$

Retaining the same notation as in [2], we write the kinetic energy of the combined system in the form

$$T = \frac{1}{2}I\dot{\sigma}^2 + \frac{1}{2}m_0\dot{v}^2 + \frac{1}{2}\rho S\sum_{i,j,m,n} a_{ijmn}\dot{q}_{ij}^{c,s}\dot{q}_{mn}^{c,s}. \tag{2}$$

Here I is the moment of inertia of the motor shaft, m_0 is the mass of the tank plus the liquid, and a_{ijmn} denotes nonlinear functions of $q_{mn}^{c,s}(t)$ [9, 11].

The potential energy of the displacements of the free surface of the liquid is equal to [9]

$$V = \rho\int_S\int dS\int_0^{\eta}(g+\dot{v})x\,dx = -\frac{1}{2}\rho S(g+\dot{v})\sum_{i,j} q_{ij}^{c,s}\,q_{ij}^{c,s}, \tag{3}$$

where g is the free-fall acceleration.

The Lagrangian of the system therefore acquires the form [8, 10]

$$L = \frac{1}{2}I\dot{\sigma}^2 + \frac{1}{2}m_0x_0^2\dot{\sigma}^2\sin^2\sigma + \frac{1}{2}\rho S\sum_{i,j,m,n} a_{ijmn}\dot{q}_{ij}^{c,s}\dot{q}_{mn}^{c,s} + \frac{1}{2}\rho Sx_0(\dot{\sigma}^2\cos\sigma + \dot{\sigma}\sin\sigma)\sum_{i,j} q_{ij}^{c,s}q_{ij}^{c,s} - \frac{1}{2}\rho Sg\sum_{i,j} q_{ij}^{c,s}q_{ij}^{c,s}. \tag{4}$$

As a result, we obtain the following Lagrangian equations for $\sigma(t)$:

$$I\ddot{\sigma} = -2m_0x_0^2\dot{\sigma}^2\sin\sigma\cos\sigma - m_0x_0^2\ddot{\sigma}\sin^2\sigma + x_0\rho S(\dot{\sigma}^2\sin\sigma - \ddot{\sigma}\cos\sigma)\times \sum_{i,j} q_{ij}^{c,s}q_{ij}^{c,s} - 2x_0\rho S\dot{\sigma}\cos\sigma\sum_{i,j} q_{ij}^{c,s}q_{ij}^{c,s} + \Phi(\sigma) - H(\sigma). \tag{5}$$

The last two terms on the right-hand side of Eq. (5) describe the driving torque and the internal friction torque of the motor. Let the shaft rotation speed $\dot{\sigma}(t)$ in steady-state operation of the motor be close to $2\omega_1$, where ω_1 is the natural frequency of

TABLE 1

Value of the parameter N_1	Type and brief description of steady state
2.25 — 2.04	Half-wave limit cycle
2.03 — 1.91	Full-wave limit cycle
1.9 — 1.88	Two-wave limit cycle
1.87	Four-wave limit cycle
1.85 — 1.81	Full-wave chaos with two windows
1.8 — 1.66	Half-wave chaos with two windows
1.65	Four-wave limit cycle
1.64	Half-wave chaos with two windows
1.55 — 1.51	Half-wave limit cycle
1.5 — 1.48	Full-wave limit cycle
1.47 — 1.46	Two-wave limit cycle
1.45	Four-wave limit cycle
1.44	Eight-wave limit cycle
1.43 — 1.37	Half-wave chaos with two windows
1.36 — 1.12	Full-wave chaos with two windows
1.11 — 0.9	Continuous chaos
0.89 — 0.35	Half-wave chaos with two windows
0.34	Two-wave limit cycle

the fundamental of the free surface oscillations, which corresponds to modes $q_{11}^c(t)\kappa_{11}(r)\cos\theta$ and $q_{11}^s(t)\kappa_{11}(r)\sin\theta$.

We now introduce the small positive parameter

$$\varepsilon = \sqrt{(x_0\omega_1^2)/g}. \tag{6}$$

We also assume that

$$\dot{\sigma} - 2\omega_1 = \varepsilon^2\omega_1\nu. \tag{7}$$

We approximate the oscillations of the free surface of the liquid by oscillations in the fundamental and second modes [11], specifying their amplitudes in the form

$$\begin{aligned} q_{11}^c(t) &= \varepsilon\lambda\left[p_1(\tau)\cos\frac{\sigma}{2} + q_1(\tau)\sin\frac{\sigma}{2}\right];\\ q_{11}^s(t) &= \varepsilon\lambda\left[p_2(\tau)\cos\frac{\sigma}{2} + q_2(\tau)\sin\frac{\sigma}{2}\right];\\ q_{01}(t) &= \varepsilon^2\lambda\left[A_{01}(\tau)\cos\sigma + B_{01}(\tau)\sin\sigma + C_{01}(\tau);\right.\\ q_{21}^{c,s}(t) &= \varepsilon^2\lambda\left[A_{21}^{c,s}(\tau)\cos\sigma + B_{21}^{c,s}(\tau)\sin\sigma + C_{21}^{c,s}(\tau)\right]. \end{aligned} \tag{8}$$

Here τ is slow time, $\tau = \varepsilon^2\sigma/4$. Determining the dimensionless amplitudes $A_{ij}^{c,s}(\tau)$, $B_{ij}^{c,s}(\tau)$, and $C_{ij}^{c,s}(\tau)$, of the second modes by Miles' method [3, 11, 12, 13] in terms of the amplitudes $p_1(\tau)$, $q_1(\tau)$, $p_2(\tau)$, and $q_2(\tau)$ and invoking the Lagrangian averaging procedure over the explicitly occurring fast time $\sigma(t)$, we obtain a system of equations for the amplitudes of the dominant modes:

$$\begin{aligned}
\frac{dp_1}{d\tau} &= -\alpha p_1 - (\nu + AE - 2)q_1 + BM p_2;\\
\frac{dq_1}{d\tau} &= -\alpha q_1 - (\nu + AE + 2)p_1 + BM q_2;\\
\frac{dp_2}{d\tau} &= -\alpha p_2 - (\nu + AE - 2)q_2 + BM p_1;\\
\frac{dq_2}{d\tau} &= -\alpha q_2 + (\nu + AE + 2)p_2 + BM q_1;\\
\frac{d\nu}{d\tau} &= N_2 - N_1\nu - \mu(p_1q_1 + p_2q_2).
\end{aligned} \tag{9}$$

The last equation in the system (9) is obtained from the equation for the speed of rotation of the shaft $\dot{\sigma}$ (5) after the averaging procedure has been applied and with the use of relations (7) and (8). Moreover, in the system of equations (9) α denotes the coefficient of additional damping forces [3, 11-13] acting on the liquid oscillations,

$$E = \frac{1}{2}(p_1^2 + q_1^2 + p_2^2 + q_2^2);$$

$$M = (p_1q_2 - p_2q_1);\ N_2 = \frac{1}{\omega_1}(N_0 - 2N_1\omega_1);\ \mu = \frac{\rho S\lambda}{(2I + m_0x_0^2)\omega_1^2 k_{11}^2};$$

N_0 and N_1 are constants of the linear static performance curve of the motor [3], k_{11} is the eigenvalue corresponding to the frequency ω_1, and A and B are constants, whose values depend on the diameter of the tank and the depth to which it is filled with the liquid [3, 12].

We have carried out a large series of numerical experiments in the parameter space of the system of equations (9) to plot the attractors of this system and to determine their quantitative and qualitative characteristics. We have devoted special attention to the detection of regions in which chaotic attractors exist for the system of equations (9). The details of the numerical procedure are described in [3]. Here we give certain results obtained in the numerical experiments.

We assume that the basic parameters and initial conditions of the system (9) are

$$\begin{aligned}
&\alpha = 0{,}8;\ A = 1{,}12;\ B = -1{,}531;\ N_2 = -0{,}25;\ \mu = 4{,}5;\\
&p_1 = (0) = q_1(0) = 0{,}1;\ \nu(0) = 0;\ p_2(0) = q_2(0) = 1.
\end{aligned} \tag{10}$$

The parameter N_1, which characterizes the slope of the performance curve of the motor, is adopted as the bifurcation parameter. The choice of N_1 as the bifurcation parameter enables us to investigate the influence of energy losses in the excitation source on the dynamics of the free surface oscillations of the liquid.

Table 1 shows the types of attractors of the system (9) that are encountered as the parameter N_1 is varied in the range $0.3 \le N_1 \le 2.25$.

We now analyze the results in Table 1 in detail.

As N_1 is varied in the interval $2.04 \le N_1 \le 2.25$, a stable, half-wave limit cycle exists in the system, but becomes unstable at $N_1 = 2.03$.

At this value of N_1 the system acquires a full-wave limit cycle as the result of a period-doubling bifurcation.

Two-wave and four-wave limit cycles are generated in the system at the points $N_1 = 1.9$ and $N_1 = 1.87$ as a result of further period-doubling bifurcations. The period-doubling bifurcation process terminates at the critical point $N_1 = 1.85$ with the emergence of a chaotic attractor, whose phase portrait is shown in projection onto the p_2q_2 plane in Fig. 2a. The transition from regular to chaotic motions adheres strictly to the Feigenbaum scenario.

The power spectrum $\log S(\Omega)$ (where Ω is the spectral frequency) [7] of the chaotic attractor at $N_1 = 1.85$ is shown in Fig. 2b. The principal Lyapunov exponent of this attractor is equal to 0.08. The chaotic attractor has a full-wave structure with

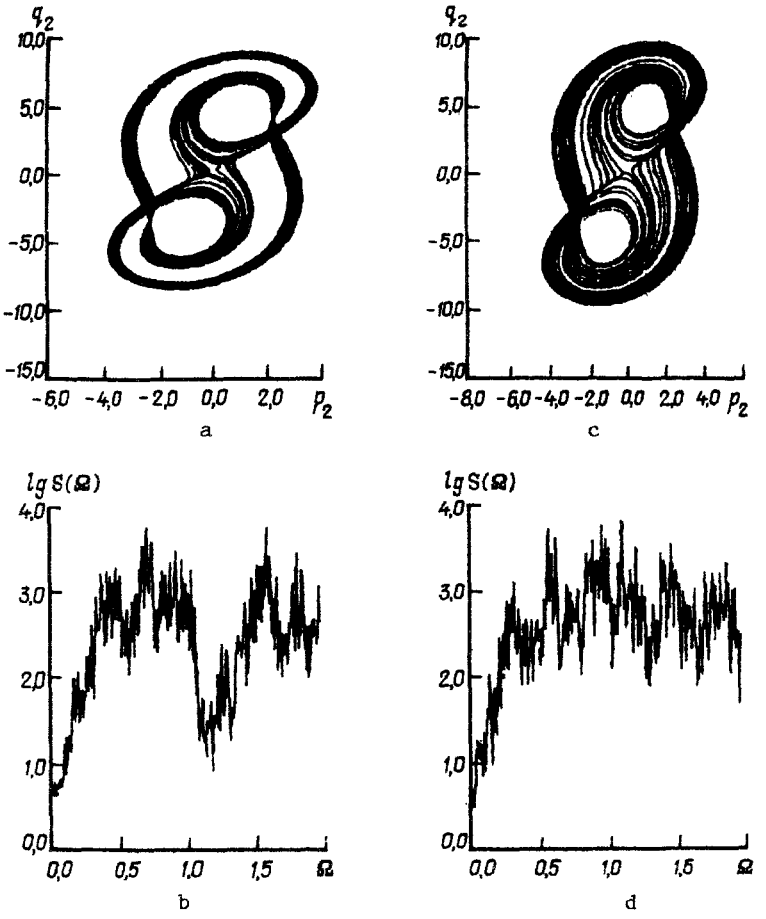

Fig. 2

two internal "windows." This type of chaotic attractor structure is observed as N_1 is varied in the interval $1.81 \leq N_1 \leq 1.85$. The full-wave tapes of the attractor then merge into a half-wave tape as a result of internal bifurcations of the chaotic attractors. This merging takes place at $N_1 = 1.8$. The projection of the phase portrait of this chaotic attractor onto the p_2q_2 plane is shown in Fig. 2c. It is evident from Fig. 2c that the half-wave chaos tape still has two internal windows. The power spectrum of the chaotic attractor at $N_1 = 1.8$ is shown in Fig. 2d. In contrast with the spectral characteristic of the preceding case, the trough in the middle-frequency part of the curve no longer exists. The principal Lyapunov exponent of the chaotic attractor (Fig. 2c) is equal to 0.14. The chaotic attractor preserves the given structure as the parameter N_1 is varied in the interval $1.66 \leq N_1 \leq 1.8$. However, as N_1 is varied between the above-indicated limits wherein the structure of the projections of the phase portraits remains constant (half-wave with two windows), they undergo certain evolutions as a result of internal bifurcation phenomena. As the values of N_1 are decreased, the attractor becomes increasingly randomized in the sense that the trajectories begin to fill up the phase volume with ever-increasing density, decreasing the area of the window in the p_2q_2-projection. The amplitudes of all the functions p_i, q_i, and ν are observed to increase in this case, as do the values of the principal Lyapunov exponents. Birth-and-death bifurcations of a great many limit cycles are observed in the system within the comparatively narrow interval $1.66 < N_1 < 1.65$, culminating in the emergence of a four-wave limit cycle in the system at $N_1 = 1.65$. Then at $N_1 = 1.64$ the system again acquires a chaotic attractor, which has a half-wave, two-window structure. The transition from steady-state regular motion to steady-state chaotic motion now takes place through intermittency [1]. This chaotic attractor again has a half-wave structure with two windows. In contrast with the preceding case, however, the principal Lyapunov exponent now increases to a value of 0.5. This indicates an increase in the rate of divergence of nearby phase trajectories of the attractor.

The detailed investigation of the bifurcations of the system are continued, beginning with $N_1 = 1.55$, at which a stable limit cycle exists in the system. A cascade of period-doubling bifurcations of the limit cycles then begins anew as N_1 is further reduced. It is evident from Table 1 that one-, two-, four-, and eight-wave limit cycles are generated in the system at the points $N_1 = 1.5$, $N_1 = 1.47$, $N_1 = 1.45$, and $N_1 = 1.44$. The cascade of period-doubling bifurcations terminates at the critical point

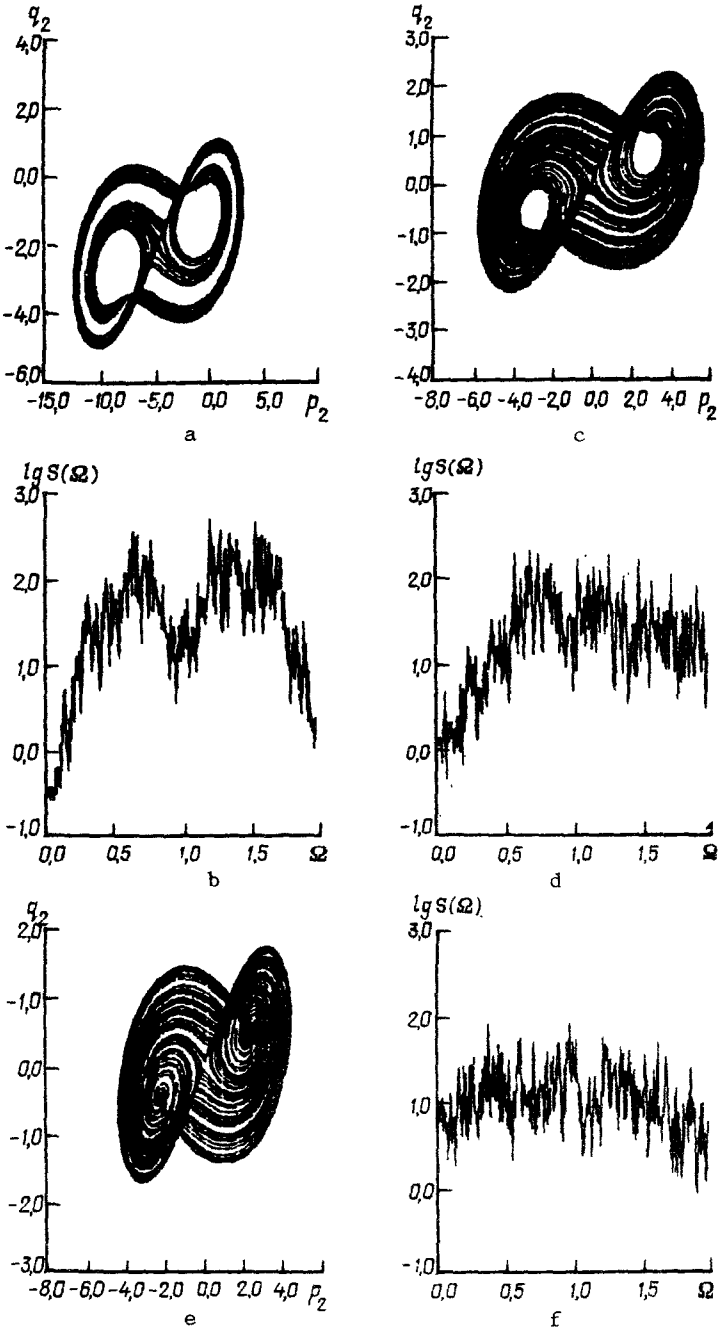

Fig. 3

$N_1 = 1.43$ with the generation of a chaotic attractor. As before, the transition from regular to chaotic motions takes place in accordance with the Feigenbaum scenario. The projection of the phase portrait of the chaotic attractor onto the p_2q_2 plane and the power spectrum for $N_1 = 1.4$ are shown in Figs. 3a and 3b, respectively.

The projection of the phase portrait of this attractor has the structure of a full-wave tape with two internal windows. The chaotic attractor has such a structure in the interval $1.37 \leq N_1 \leq 1.43$. Then as N_1 is further decreased, internal bifurcations of the chaotic attractors are observed in the system. For example, the full-wave tape of the attractor merges into a half-wave tape at the point $N_1 = 1.36$. The projection of the phase portrait of the chaotic attractor onto the p_2q_2 plane and the power spectrum of the chaotic attractor with this structure at $N_1 = 1.25$ are shown in Figs. 3c and 3d, respectively. Subsequent internal homoclinic bifurcations lead to the generation of a chaotic attractor having a half-wave continuous structure, i.e., chaos with the most fully developed randomization. This type of chaotic attractor exists as N_1 is varied in the interval $0.9 \leq$

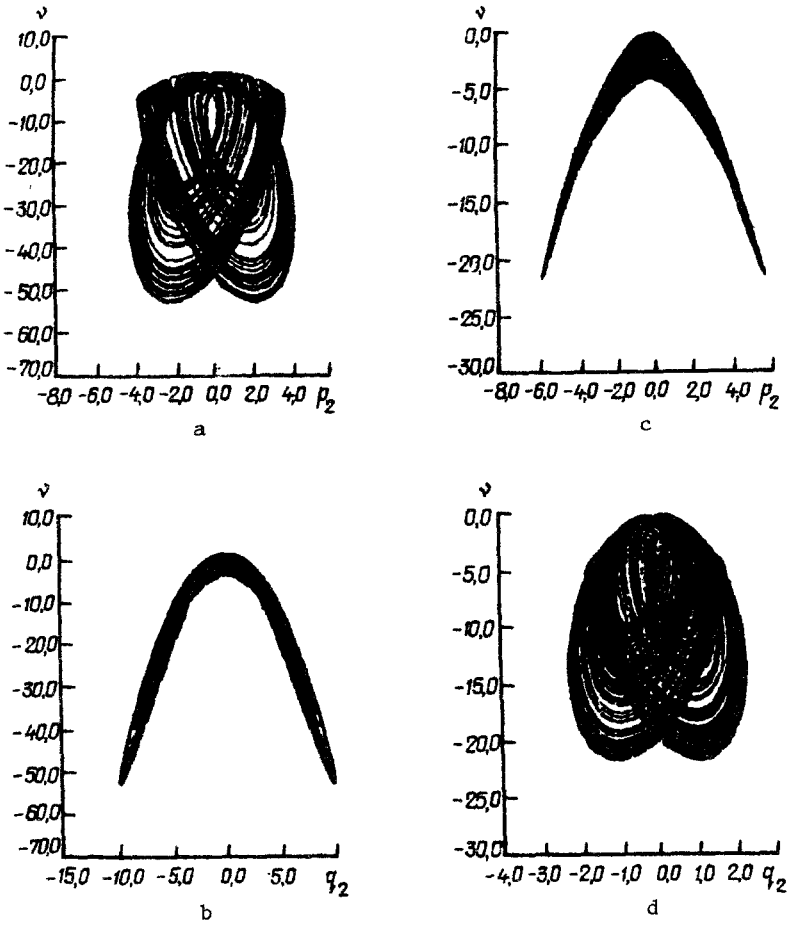

Fig. 4

$N_1 \leq 1.11$. The projection of the phase portrait of the chaotic attractor onto the p_2q_2 plane and the power spectrum of this type of chaotic attractor at $N_1 = 1.05$ are shown in Figs. 3e and 3f, respectively. At $N_1 = 0.89$ the system once again acquires a chaotic attractor with a half-wave, two-window structure. This chaotic attractor structure exists for $0.35 \leq N_1 \leq 0.89$. At $N_1 = 0.34$ the chaotic attractor is superseded by a regular two-wave limit cycle.

We note that the structural differences of the attractors are well illustrated not only by the projections of the phase portraits, but also by their spectral characteristics shown in Figs. 3b, 3d, and 3f. For example, full-wave chaos has distinct troughs at low and middle frequencies. Half-wave, two-window chaos, in turn, has only a low-frequency trough, and the structure of half-wave continuous chaos resembles a continuous noise plateau.

It is instructive to investigate the variation of such an important quantitative characteristic of the chaotic state as the principal Lyapunov exponent for the various types of chaotic attractors. We have established the fact that the Lyapunov exponent increases with the evolution of a chaotic attractor. For example, the principal Lyapunov exponent $\lambda_1 = 0.08$ at $N_1 = 1.4$. This exponent then becomes equal to 0.14 for half-wave, two-window chaos at $N_1 = 1.25$. The value of λ_1 increases to 0.2 for continuous chaos at $N_1 = 0.5$. The exponent λ_1 subsequently decreases to 0.12 at $N_1 = 0.5$. The dynamics of the variation of the principal Lyapunov exponent is fairly typical. It indicates an increase in the rate of divergence of nearby phase trajectories for more randomized chaotic attractors.

We also consider a very significant aspect of the problem. It follows from our investigations that the different types of chaotic attractors existing in the system of equations (9) as N_1 is varied in the interval $1.64 \leq N_1 \leq 1.85$ have a great deal in common with the corresponding types of chaotic attractors that exist in the system as the parameter N_1 is varied in the interval $0.35 \leq N_1 \leq 1.43$. This commonality is manifested both in the structure of the corresponding projections of the phase portraits and in the similarity of the spectral characteristics. However, there is one major difference, which we illustrate in the example of a half-wave, two-window attractor.

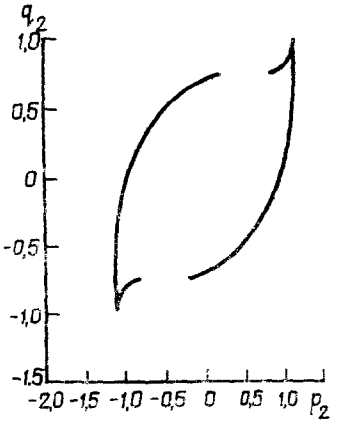

Fig. 5

Figures 4a and 4b show the projections of the phase portrait of the chaotic attractor constructed at $N_1 = 1.8$ onto the $p_2\nu$ and $q_2\nu$ planes, respectively. Figures 4c and 4d show the same projections for the chaotic attractor constructed at $N_1 = 1.25$. It is evident from these figures that the projection of the phase portrait of the chaotic attractor constructed at $N_1 = 1.8$ onto the $p_2\nu$ plane is structurally similar to the projection of the phase portrait of the chaotic attractor constructed at $N_1 = 1.25$ onto the $q_2\nu$ plane. Conversely, the projection of the phase portrait of the first attractor onto the $q_2\nu$ plane is structurally similar to the projection of the phase portrait of the second attractor onto the $p_2\nu$ plane.

It has been established on the basis of our investigations that the corresponding projections for other types of chaotic attractors will exhibit the same kind of similarity.

Consequently, the projections of the phase portraits of chaotic attractors existing in the interval $1.64 \leq N_1 \leq 1.85$ onto the $p_2\nu$ and $p_1\nu$ planes are structurally similar to the projections of the phase portraits of the corresponding types of attractors existing in the interval $0.35 \leq N_1 \leq 1.43$ onto the $q_2\nu$ and $q_1\nu$ planes. Conversely, the projections of the phase portraits of chaotic attractors in the interval $N_1 \in (1.64, 1.85)$ onto the $q_2\nu$ and $q_1\nu$ planes are structurally similar to the projections of the phase portraits of the chaotic attractors in the interval $N_1 \in (0.35, 1.43)$ onto the $p_2\nu$ and $p_1\nu$ planes.

Another similarity between the projections of the phase portraits both for regular and for chaotic attractors is associated with the symmetry of the system of equations (9) with respect to the variables p_1, q_1 and p_2, q_2. As a consequence of this symmetry, the projection of the phase portrait onto the p_1q_1 plane coincides with the projection onto the p_2q_2 plane to within a constant factor in any steady state, either regular or chaotic.

Finally, we note that the Poincaré sections of all the chaotic attractors have a tape structure. As a typical illustration of this kind of structure, Fig. 5 shows the p_2q_2-projection of the Poincaré section of the chaotic attractor constructed at $N_1 = 1.4$ in the plane $\nu = -1.5$.

Special emphasis must be given to the fact that the chaotic attractors are typical steady states of the investigated dynamical system. It follows from the results in Table 1 that the parameter N_1 has rather large intervals in which chaotic attractors exist. We have also investigated the bifurcations of the system of equations (9) as the parameters α and N_2 are varied. These investigations have disclosed the existence of fairly large intervals of α and N_2 in which the system (9) has chaotic attractors. We have established the fact that the regions of existence of chaotic attractors occupy large domains in the parameter space of the system of equation (9).

We close with the observation that we have compared the results for the cases of ideal and nonideal excitation of oscillations of the free surface of the liquid. The system of equations for ideal excitation are readily obtained from the system (9). The fifth equation in the system (9) needs to be discarded for ideal excitation, and ν must be regarded as a given constant rather than an unknown function in the other four equations. This transformation renders the system of equations numerically integrable for the same values of A, B, and α and for the same initial values as in (10). The value of ν is varied in the interval $(2\nu_1, 2\nu_2)$, where ν_1 and ν_2 are the minimum and maximum amplitudes, respectively, of the detuning oscillations for steady states in the case of nonideal excitation. The corresponding computations are carried out with very small increments of the detuning ν. It has been established that stable equilibrium positions are the only attractors of the given system of equations for those parameters so chosen in the ideal excitation case. Consequently, "ideal" computational models yield incorrect results for the

excitation of oscillations by a source of limited power, because entire classes of steady states, including the chaotic kind, become undetectable.

We have thus arrived at the following main results in an investigation of the nonlinear interaction of the dynamical system {liquid in tank + electric motor}. We have proved the existence of chaotic attractors of the investigated dynamical system in parametric oscillations. We have confirmed that the transition from regular to chaotic motions can take place either by the Feigenbaum scenario or through intermittency. We have investigated the bifurcations of chaotic attractors. We have described in detail the quantitative and qualitative characteristics of various types of chaotic attractors existing in the system.

REFERENCES

1. V. S. Anishchenko, Complex Oscillations in Simple Systems [in Russian], Nauka, Moscow (1990).
2. P. S. Koval'chuk and T. S. Krasnopol'skaya, "Resonance effects associated with nonlinear oscillations of cylindrical shells with initial imperfections," Prikl. Mekh., **15**, No. 9, 100-107 (1979).
3. T. S. Krasnopol'skaya and A. Yu. Shvets, "Properties of chaotic oscillations of a liquid in cylindrical tanks," Prikl. Mekh., **28**, No. 6, 52-58 (1992).
4. V. D. Kubenko, P. S. Koval'chuk, and T. S. Krasnopol'skaya, Nonlinear Interaction between Flexural Modes of Cylindrical Shells [in Russian], Naukova Dumka, Kiev (1984).
5. S. Ciliberto and J. P. Gollub, "Chaotic mode competition in parametrically forced surface waves," J. Fluid Mech., **158**, 381-398 (1985).
6. J. D. Crawford and E. Knobloch, "Symmetry and symmetry-breaking bifurcations in fluid dynamics," Ann. Rev. Fluid Mech., **23**, 341-387 (1991).
7. T. Kambe and M. Umeki, "Nonlinear dynamics of two-mode interaction in parametric excitation of surface waves," J. Fluid Mech., **139**, 461-471 (1990).
8. E. Meron and J. Procaccia, "Low-dimensional chaos in surface waves: theoretical analysis of an experiment," Phys. Rev. A, **34**, 3221-3237 (1986).
9. J. W. Miles, "Nonlinear surface waves in closed basins," J. Fluid Mech., **75**, 419-448 (1979).
10. J. W. Miles, "Resonant motion of a spherical pendulum," Physica D, **11**, 309-323 (1984).
11. J. W. Miles, "Nonlinear Faraday resonance," J. Fluid Mech., **146**, 285-302 (1984).
12. J. W. Miles, "Resonantly forced surface waves in circular cylinder," J. Fluid Mech., **149**, 15-31 (1984).
13. J. W. Miles and D. Henderson, "Parametrically forced surface waves," Ann. Rev. Fluid Mech., **22**, 143-165 (1990).